

Hydrogen-Bonding-Driven Complexation of Polystyrene-*block*-poly(ethylene oxide) Micelles with Poly(acrylic acid)

Shuguang Yang,[†] Xinfei Yu,[†] Lian Wang,[‡] Yingfeng Tu,[†] Joseph X. Zheng,[†] Junting Xu,[‡] Ryan M. Van Horn,[†] and Stephen Z. D. Cheng*,[†]

[†]Department of Polymer Science, College of Polymer Science and Polymer Engineering, The University of Akron, Akron, Ohio 44325-3909, and [‡]Department of Polymer Science, Zhejiang University, Hangzhou 310027, China

Received December 16, 2009; Revised Manuscript Received February 18, 2010

ABSTRACT: Hydrogen-bonding complexation between spherical diblock copolymer polystyrene-*block*-poly(ethylene oxide) (PS-*b*-PEO) micelles and poly(acrylic acid) (PAA) was systematically investigated. We prepared the micelles by gently adding a selective solvent, water, to a PS₂₄₀-*b*-PEO₁₈₂/N,N-dimethylformamide (DMF) solution. After DMF was removed by dialysis, the diluted micelles were associated with PAA at different pH values. The complexation behavior was studied via ultraviolet-visible spectroscopy, laser light scattering, ζ -potential, and transmission electron microscopy techniques. As the pH value varied, the complexation between the PS₂₄₀-*b*-PEO₁₈₂ micelles and PAA behaved differently. At pH < 3.0, the system was in the flocculation region where large aggregates of the micelles formed spontaneously. A single-micelle, stepwise adsorption region could be observed when the pH value was in the range of 3.0–4.8. Above a pH value of 4.8, no adsorption could be found. The value of pH 3.0 was recognized as the onset pH value for the micellar flocculation. At this value, the micelle flocculating rate was very slow, and thus the flocculating process was able to be monitored. A “pearl-necklace-like” morphology at pH 3.0 was observed, and its formation mechanism was also discussed.

Introduction

A micelle is a submicroscopic self-assembly of molecules with different hierarchical structures. Micellization of small amphiphilic molecules, such as surfactants and liposomes, is a classic topic of colloid and interface science. Different than small amphiphilic molecules, block copolymers have larger sizes and slower mobility; therefore, their micellization process may be much more complicated and does not necessarily reach the equilibrium state. In the last two decades, micellization behavior of block and graft copolymers has been widely investigated, including aggregation mechanisms, kinetics of morphological changes, intermediate morphological states, and various applications.^{1–6}

These developments have greatly benefited from the synthesis block copolymers with well-defined compositions, controlled molecular weights and distributions, and designed chemical structures using living ionic or controlled radical polymerizations. Micelles can serve as building blocks to self-assemble further or associate with other macromolecules to construct structural hierarchies. For example, spherical micelles can closely pack into face-centered cubic or hexagonal close-packed structures, and cylindrical micelles can form a 2D hexagonal phase at high concentrations in solution.^{7,8} In this publication, we will discuss an additional method of creating structural hierarchy using micelles associated with other macromolecules via hydrogen-bonding complexation, specifically, using diblock copolymer micelles of polystyrene-*block*-poly(ethylene oxide) (PS-*b*-PEO) associated with poly(acrylic acid) (PAA).

Hydrogen-bonding complexation in polymers was first reported as early as 1948 by Dorby.⁹ In the 1960s, researchers at

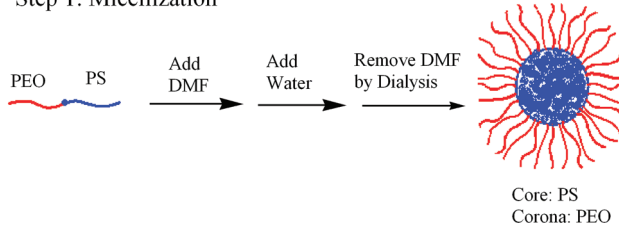
Union Carbide systematically studied hydrogen-bonding complexation of PEO and PAA.^{10,11} Tsuchida et al. summarized the research activities on hydrogen-bonding complexation in polymers from the 1950s to the beginning of the 1980s.¹² Jiang et al. have also provided a thorough review of this topic.¹³ Recently, the hydrogen-bonding association was introduced to the process of micellization of block copolymers.^{14–19} Chen et al. described a controllable vesicle formation of a block copolymer PEO-*b*-polybutadiene (PB) complexing with PAA with a molecular weight of 2000 g/mol in a solvent mixture of THF and *n*-dodecane.¹⁴ In this case, THF is a cosolvent for PEO, PB blocks, and homopolymer PAA, whereas *n*-dodecane is a selective solvent for PB blocks. In addition to micellization when *n*-dodecane was added, the PEO blocks and the PAA can form hydrogen-bonded association. Zhang et al. discussed the combination of micellization and hydrogen-bonding association using a laser light scattering (LLS) technique on the systems of PS-*b*-PAA/PS-*b*-PEO and PS-*b*-PAA/PMMA-*b*-PEO mixtures in toluene.^{16,17} Bokias et al. studied complexation behavior between stimuli-responsive triblock copolymer PEO-*b*-poly(2-vinylpyridine)-*b*-PEO and PAA and reported star-like and flower-like micelles.¹⁸

Thermodynamic analysis of the combinations of classic micellization and interpolymer complexation is usually difficult because these systems are composed of multiple components such as block copolymer, homopolymer, common solvent, and selective solvent. However, combinations of the structural formations usually lead to observations of different hierarchical structures. In biorelated systems, multiple-hierarchical structures are the key for proteins or DNAs to realize their biofunctionality. Understanding how proteins fold or how DNAs spiral to form multiple-hierarchical structures is one of the most important

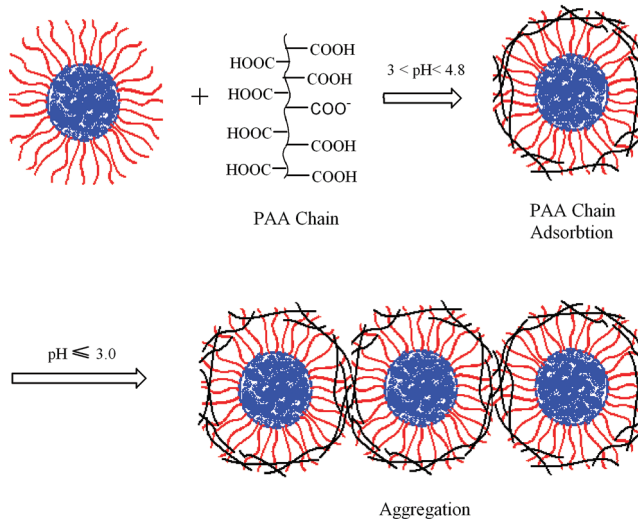
*To whom the correspondence should be addressed. E-mail: scheng@uakron.edu.

Scheme 1. Separated Micellization and Complexation Process

Step 1: Micellization



Step 2: Hydrogen Bonding Complexation



tasks in biochemistry and biophysics. Adopting synthetic polymers as model compounds to study chain associations based on secondary interactions, such as hydrogen-bonding, can provide useful information about multiple-hierarchical structure formations.

To simplify the study in this publication, we sequentially separated micellization and the interpolymer hydrogen-bonding complexation processes into two steps: first, we prepared diblock copolymer spherical micelles from a PS-*b*-PEO sample with an average degree of polymerization of 240 in the PS block and 182 in the PEO blocks (PS_{240} -*b*- PEO_{182}) in DMF/water solution systems. Then, we removed DMF by dialysis and let the micelles associate with PAA at different pH values. These two steps are shown in Scheme 1.

Experimental Section

Materials. Anhydrous DMF was purchased from Acros (water content < 50 ppm). PAA with a molecular weight of ~50 000 g/mol in a 25 wt % water solution was purchased from Polysciences, Inc. A low-molecular-weight PAA (5700 g/mol, PDI 1.09, purchased from Polymer Source) was also used to check the possible molecular weight dependence on the complexation and aggregate morphology. The diblock copolymer of PS-*b*-PEO was synthesized using living anionic polymerization based on a standard route, which was published elsewhere.²⁰ The number-average molecular weight PS precursor was characterized by size exclusion chromatography (SEC) using polystyrene standards, and then, the number-average molecular weight of the PEO blocks was determined by proton nuclear magnetic resonance (¹H NMR). The diblock polymer is denoted as PS_{240} -*b*- PEO_{182} according to the average degree of polymerization for each block. The overall polydispersity of PS_{240} -*b*- PEO_{182} determined by SEC using the universal calibration was

1.08. The volume fraction of the PS blocks (f_V^{PS}) was 0.769 based on the density data from refs 21 and 22.

Micelle Preparation. The diblock copolymer PS_{240} -*b*- PEO_{182} was first dissolved in anhydrous DMF by stirring at room temperature for a few days to obtain stock solutions of the required copolymer concentration (1.33 mg/mL). Anhydrous DMF was prefiltered by 0.02 μm pore size filters (Whatman Anotop 25, 0.02 μm) before making the stock solutions. The solution was then sealed with Teflon tape and stored at room temperature for future preparation of micelles. Deionized (DI) water was then added drop by drop at a very slow rate (0.5 wt % per hour) into the PS_{240} -*b*- PEO_{182} /DMF solutions under magnetic stirring until the overall water volume content was 25 wt %. After the addition of water, the solution (stock solution) was kept stirring at room temperature for 2 to 3 days. Finally, the solution was dialyzed against DI water to remove the DMF.

Micelles Associated with PAA at Different pH Values. The dialyzed micelle solution was diluted in different pH aqueous solutions to the concentration of 1:10, 1:20, 1:50, or 1:100 of the stock micelle solution. The pH values were adjusted by hydrochloric acid (HCl) and monitored by a pH meter (Mettler Toledo S20). PAA solutions were then added to the diluted PS_{240} -*b*- PEO_{182} micelle solution drop by drop with 1:1 molar ratio of the PEO and PAA repeating units. In the diluted micelle solution, the concentration of the block copolymer was low. We only needed to add a trace amount of PAA, and thus a small volume of PAA solution into the system. In general, the PAA solution is < 5 vol %. The PAA and water content in the PAA solution possessed very little effect on the whole system. Correspondingly, the pH value of the system only changed within the experimental error (± 0.02).

Association at pH 3.0 and Aggregation Process Monitoring. Three approaches were applied to induce association between micelles and PAA: (1) dilution of the stock micelle solution with a pH value of 3.0 and then under magnetic stirring, adding PAA solution slowly drop by drop (this process is symbolized as pH3-Micelles-PAA); (2) dilution of the PAA solution at pH 3.0 and then under magnetic stirring, adding dialyzed stock micelle solution drop by drop (this process is symbolized as pH3-PAA-Micelles); and (3) dilution of the PAA and micelles in the neutral DI water at the same time and then adjusting the pH value to 3.0 by titration (this process is symbolized as Micelles-PAA-pH3).

Equipment and Experiments. The morphological observations were performed on a transmission electron microscope (TEM Philips TECNAI) with an accelerating voltage of 120 kV. To observe micelle morphologies, the original micelle solution was diluted 20 times; then, a drop of the diluted solution was placed on a Formvar/carbon-coated grid. After a few minutes, the excess solution was blotted away with filter paper. The grids were dried at room temperature and atmospheric pressure for several hours before examination in the TEM.

LLS experiments were conducted using a Brookhaven Instrument coupled to a BI-200SM goniometer, a BI-9000AT correlator, and an EMI-9863 photomultiplier tube for photon counting. A Meller Griot 35 mW He-Ne laser was used as the light source (632.8 nm). A cylindrical glass scattering cell with a diameter of 12 mm was placed at the center of a thermostatic bath (0.01 °C) with decahydronaphthalene used for refractive index matching. The solutions were filtered into the scattering cells through syringe filters of 0.45 or 1.0 μm pore size. Both the scattering intensity and hydrodynamic diameter were measured at a scattering angle of 90° and a temperature of 25 °C. For the purpose of determining size and shape of the initial micelle association at pH 3, different scattering angles in dynamic LLS were also utilized.

The ζ -potential measurement was conducted on a Malvern Instrument (Nano ZS90) equipped with a 632.8 nm He-Ne laser. The instrument calculates the ζ -potential by determining the electrophoretic mobility and applying the Henry equation.

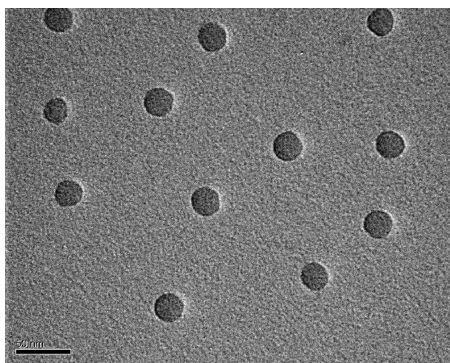


Figure 1. TEM bright field images of PS_{240} -*b*- PEO_{182} spherical micelles. The scale bar is 50 nm.

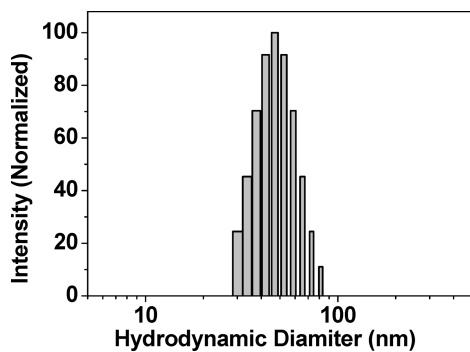


Figure 2. Hydrodynamic diameter distribution of the micelles obtained in water solution utilizing LLS experiments.

The electrophoretic mobility is obtained by performing an electrophoresis experiment on the sample and measuring the velocity of the particles using laser doppler velocimetry.

UV-visible spectra were recorded on an HP 8453 spectrometer. The spectroscopic wavelength scan range was selected from 300 to 800 nm. First, 3.0 mL of neutral water in a regular quartz cell ($1 \text{ cm} \times 1 \text{ cm}$) was measured as a blank reference. Then, 3.0 mL solutions of micelle and PAA associations at different pH values were put into the same cell and measured one by one. The measurement sequence is from high to low pH values, and after one measurement, the cell was rinsed three times with DI water before the next measurement.

Results and Discussion

Micellar Morphologies of PS_{240} -*b*- PEO_{182} Diblock Copolymers. Because DMF is a common solvent for PS and PEO, the PS_{240} -*b*- PEO_{182} sample was first dissolved in DMF. To form micelles, water was then gently added into the solutions. Because PS blocks are hydrophobic and PEO blocks are hydrophilic at room temperature, water is the selective solvent for the PEO blocks. The micelle morphologies in the system are critically dependent on factors such as lengths of the PS and the PEO blocks, the block volume fraction, the copolymer concentration, the content of added water, and the micellization temperature.^{23–27} Figure 1 shows a TEM bright field image of spherical micelles of PS_{240} -*b*- PEO_{182} from DMF/water solution with a water concentration of 25 wt %. The average diameter of the spherical micelles was measured to be 25 nm with a relatively narrow distribution. Note that the TEM observations were carried out in the solid state after the micelles had dried.

Figure 2 shows the hydrodynamic diameter and distribution of these micelles in water characterized utilizing dynamic LLS. The LLS scattering experiments provide size and

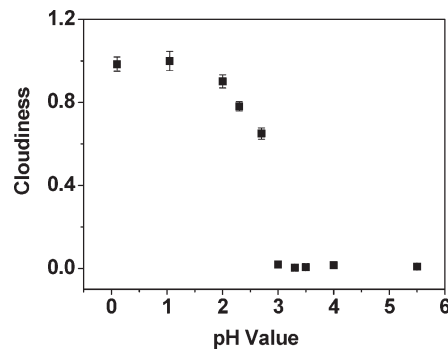


Figure 3. Normalized cloudiness of PS_{240} -*b*- PEO_{182} micelles associated with PAA as a function of pH value. The cloudiness was determined by visible spectroscopic absorbance. The micelle concentration is 1:20 of the stock solution.

morphological information (diameter, ~ 45 nm on average) based on a spherical structure (Stokes–Einstein equation).²⁸ This value should be larger than the one observed in the solid state from TEM (~ 25 nm) because of collapse after drying.

Spherical Micelles Associated with PAA at Different pH Values. The dialyzed micelle solutions were diluted to the concentration of 1:20 of the stock solution at different pH values at room temperature. Applying this condition, the concentration of the diblock copolymer is now at ~ 50 ppm. The PAA/water solution was added to the micelle solution with an equal number of PAA repeat units as the PEO blocks to match a stoichiometric proportion of hydrogen bonding. Qualitatively speaking, the solutions were cloudy at lower pH values, whereas at the higher pH values, the solutions remained transparent.

Figure 3 shows UV-visible spectroscopic results of these solutions. The average absorbance between 400 and 800 nm was used as a parameter to describe the cloudiness of the solutions. The normalized cloudiness or the normalized absorbance of PS_{240} -*b*- PEO_{182} micelles associated with PAA was plotted as a function of pH value. As shown in this Figure, when the pH value was reduced below 3.0, the solution cloudiness dramatically increased. This sudden increase in the solution cloudiness must be attributed to the occurrence of flocculation. If this deduction is true, then the value of pH 3.0 could thus be identified as an onset pH value for flocculation.

We know that flocculation of micelles after the PAA association generates large aggregates, and they can easily be filtered out from solution. To prove further that this is the onset of flocculation, we filtered the micelles after the PAA association at different pH values using two types of syringe filters with 0.45 and $1.0 \mu\text{m}$ filtration sizes. These filtered solutions were then characterized by LLS. The scattering intensity as a function of pH value is shown in Figure 4a. At $\text{pH} < 3.0$, the scattering intensity was independent of the filtration size and was close to the pure solvent. This indicates that at $\text{pH} < 3.0$, the aggregates formed by the flocculation of these micelle/PAA complexes were removed by the filters with both filtration sizes. At $\text{pH} 3.0$, the scattering intensity is still identical to those values at $\text{pH} < 3.0$ when the $0.45 \mu\text{m}$ filter was used. The scattering intensity becomes stronger when the $1.0 \mu\text{m}$ filter was used. This reveals that after 3 days, the micelles formed small aggregates that can pass through the $1.0 \mu\text{m}$ filter but not the $0.45 \mu\text{m}$ filter. When the solutions with $\text{pH} > 3$ were filtered by both 0.45 and $1.0 \mu\text{m}$ filtration sizes, all of them exhibited strong scattering intensities, indicating that the micelles are individually associated with PAA, yet no flocculation occurs when the solution pH is > 3.0 .

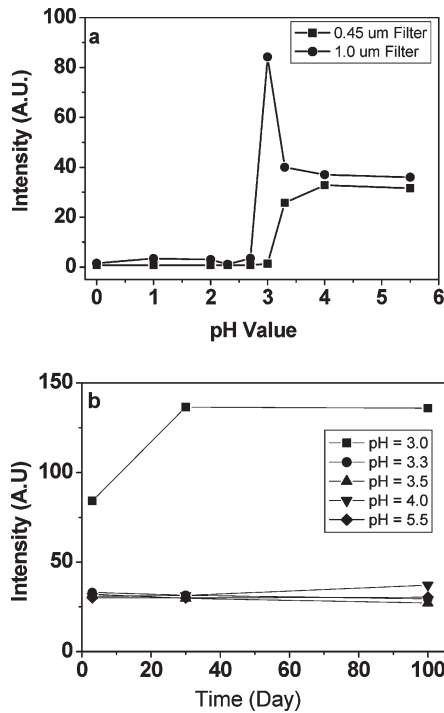


Figure 4. Scattering intensity of the complexation of PS_{240} -*b*- PEO_{182} micelles and PAA at different pH values: (a) filtered by different size filter (after 3 days) and (b) monitored at different times (filtered by 1.0 μm filter).

The micelles associated with PAA at $\text{pH} \geq 3.0$ were monitored at different times after PAA was added to the solutions. Figure 4b shows the LLS results for the systems at pH values of 3.0, 3.3, 3.5, 4.0, and 5.0, respectively, for the diblock copolymer concentration controlled at 50 ppm. When $\text{pH} > 3.0$, all of the systems provide almost identical scattering intensities for a very long period of time (up to 100 days), indicating that the systems are stable and in thermodynamic equilibrium. However, at $\text{pH} 3.0$, the scattering intensity increases with time. After a month, the scattering intensity reaches a saturated value. These LLS results further demonstrate that pH 3.0 can be recognized as the onset pH value of flocculation.

On the basis of our experimental observations, the dominant factor to control this flocculation process is the pH value. For the stock solution that contains 1 mg/mL diblock copolymer when 20-times-diluted, spherical micelles associated with PAA flocculate at an onset pH value of 3.0. To slow down the flocculation kinetics, we can further dilute the micelle solution to 100 times diluted. It is expected that at the lower concentration, there is less opportunity for PAA-associated micelles to collide and form large aggregates. It thus takes a longer time to observe the aggregation.

To confirm the LLS observations, the PAA-associated solutions at different pH values were also measured using ζ -potential measurements, and the results for a micelle concentration of 1:20 of the stock solution are shown in Figure 5 as an example. Note that the micelle interfaces are generally more negatively charged.²⁹ One of the several reasons for the negative charges is that anions tend to unspecifically bind to interfaces of the micelles.²⁹ Our measurements on the ζ -potential value of the original spherical micelles dispersed in neutral water is at -16.5 mV . Starting from pH 2.3, the ζ -potential value of the PAA-associated system is close to zero. With an increase in the pH value, the ζ -potential decreases. When pH 3.0, the ζ -potential value is close to -16.5 mV . If we further increase the pH value

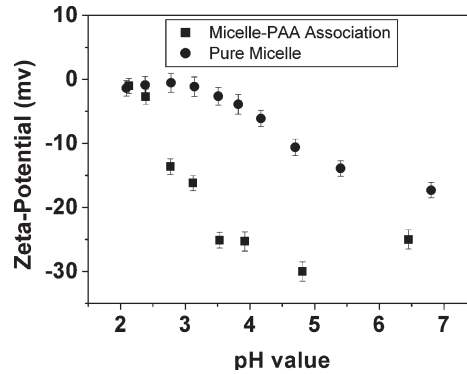


Figure 5. ζ -potential of the pure PS_{240} -*b*- PEO_{182} micelles and the complexation of the micelles and PAA as a function of pH value. The micelle concentration is 1:20 of the stock micelle solution.

to > 3.0 , the ζ -potential value continues to decrease until it reaches a minimum value at pH of ~ 4.8 , indicating that the individual micelles are stable. At this minimum, the PAA-associated micelles contain the most negative charge while balancing the interactions of the PAA adsorption and ionization. At an even higher degree of ionization or higher pH, the hydrogen bonding is dissociated, and no PAA adsorption can take place, creating a solution of free PAA molecules and individual spherical micelles.

In the same Figure, we also included the ζ -potential values of the pure micelles in water. It is evident that up to a pH value of 3.0, the values are almost a constant around a small negative value close to zero. Starting at pH 3.0, the ζ -potential continuously decreases to -17 mV at pH 7. This observation indicates that the minimum of the micelle/PAA/water system around pH 4.8 is caused by the disassociation of the PAAs from the micelles having PEO blocks as coronas. Therefore, the negative charges on the micellar surfaces gradually return to the value of the pure micelle/water system, as shown in Figure 5.

LLS and TEM experimental observations have shown that at $\text{pH} > 3.0$, there is no micellar aggregation. This indicates that at $3.0 < \text{pH} < 4.8$, there should be a region where PAA was adsorbed onto the individual micellar surface, yet the micelles did not flocculate. However, as the pH value increases to > 4.8 , the degree of ionization of PAA became $> 10\%$,^{30,31} and the interpolymer association via hydrogen bonding with PEO was prevented.^{12,32–35} By further increasing the pH value, no PAA chains can be adsorbed onto the micellar surface; therefore, no hydrogen-bonding-driven flocculation was possible.

On the basis of our experimental observations, the complexation behavior of PS_{240} -*b*- PEO_{182} micelles and PAA chains can be recognized by dividing the pH values into three regions: flocculating region, single micelle adsorption region, and nonadsorption region. Figure 6 schematically illustrates the region boundaries, and typical corresponding micellar morphologies are shown. It should be noted that the transition from one region to the other is not sharp but is represented as a boundary zone, as shown in Figure 6. From the previous discussion, pH 3.0 is recognized as the onset of flocculation; therefore, the boundary between the flocculation and single micelle adsorption region is a narrow zone centered at pH 3.0. To the direction of $\text{pH} < 3.0$, the system became increasingly flocculated; whereas, to the direction of $\text{pH} > 3.0$, they resist flocculation until dissociation occurs. The boundary zone between pH values of 4.8 and 5.6 in Figure 6 represents a gradual disappearance of the single micelle adsorption toward the nonadsorption region.

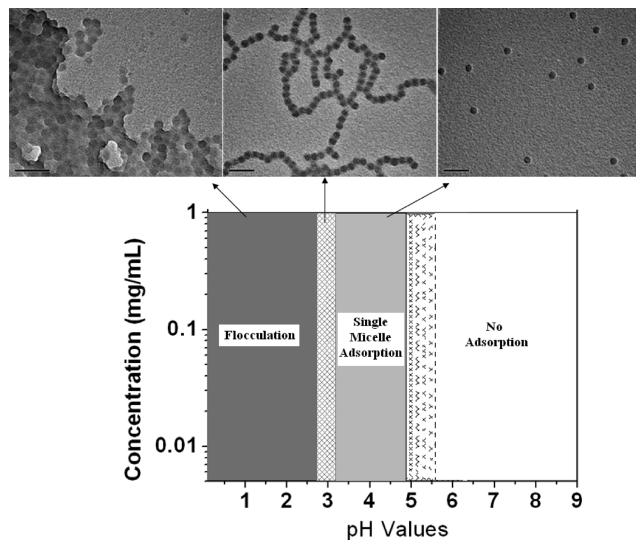


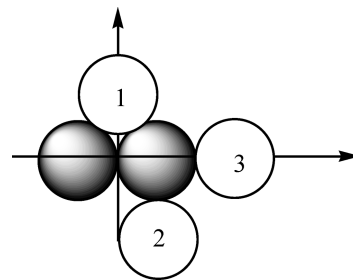
Figure 6. Divided regions of association between PS₂₄₀-*b*-PEO₁₈₂ micelles and characteristic TEM images of different regions: (left) pH 2.0, flocculation region; (middle) pH 3.0, flocculation onset point, boundary between flocculation region and single micelle adsorption region; (right) pH 4.0, single micelle adsorption region. The TEM scale bar is 100 nm. The patterned areas around pH 3.0 and 5.0 are the boundaries between the different regions.

It is worthwhile to note that these three regions observed in Figure 6 were also PAA molecular-weight-dependent when the concentration of PAA is lowered to reach a point that every PAA is absorbed on the micellar spheres. If the PAA with 5700 g/mol was used to replace the ~50 000 g/mol PAA, we need to have more molecules and thus higher concentration to retain the aggregate morphology and leave the region boundaries unchanged. This indicates that each micellar sphere requires the same number of PAA interactions with PEO blocks to control the stability of the morphology and region boundaries.

Aggregation Formation Mechanism at pH 3.0. In the flocculating region at pH values < 2.0, the process is extremely quick. It is hard to monitor experimentally the flocculation kinetics. Between the pH values of 2 and 3, the kinetics gradually slow down. For example, at pH 2.3, the flocculation took a few minutes to occur, whereas at pH 2.7, it finished within a few hours. At the onset point of pH 3.0, or within the boundary zone close to the flocculation side (slightly below 3.0), the flocculation rate is slow enough to allow us to monitor precisely the kinetics. It has been found that the spherical micelles, at first, prefer to aggregate into a “pearl-necklace-like” morphology at pH 3.0, as shown in the center TEM image of Figure 6. The formation mechanism of this aggregated morphology can be analyzed on the basis of DLVO theory, which was suggested over 60 years ago by Deryaguin and Landau and also by Vervey and Overbeck (hence the acronym DLVO).³⁶ The DLVO theory was applied to explain the tendency of colloidal particle toward either aggregation or dispersion under the simple combination of attractive van der Waals forces and repulsive electrostatic effects. In our case, there is a repulsive electrostatic force, whereas the main attractive force is hydrogen bonding.

At pH 3.0, the PAA possesses some degree of ionization due to the fact that PAA can be restrictively ionized in aqueous solution.^{30,31,37} When PAA is adsorbed onto the micelle surface (all calculations for this discussion assume that the PAA is completely adsorbed onto the PEO corona), the overall surface has some distributed negative charges. Qualitatively, these charges would prevent the micelles from

Scheme 2. Growth Mechanism of the Spherical Micelles to Form the “Pearl-Necklace-Like” Morphology



coming together to aggregate. However, if the charge repulsion is not strong enough, then thermal perturbation may overcome the repulsion barrier and achieve an aggregation of two spherical micelles. Because of the hydrogen bonding, the contacted micelles may associate with each other, forming the “nucleus” of the “pearl-necklace-like” morphology.

The schematic growth mechanism of these spherical micelles is shown in Scheme 2. If the “pearl-necklace-like” morphology can be formed, the spherical micelles prefer to aggregate at position 2 or 3 rather than position 1. To explain why position 2 or 3 is more favored for the spherical micelle aggregation compared with position 1, we need to calculate the energy barrier of each position related to both the negative charges and hydrogen bonding. Roughly speaking, position 1 has the most negative charge in contact with the neighboring micelles, and this position possesses the highest repulsion, namely, the highest energy barrier (ΔE). Hydrogen bonding is characterized to be a shorter-distance interaction, and energy falls off much quicker with distance compared with electrostatics. Although at position 1, there are more hydrogen-bonding sites available, the approaching micelle first encounters the highest energy barrier attributed to the static charge repulsion force. Therefore, the colloids have less resistance to select position 2 or 3 instead of position 1 and prefer to adsorb there. Note that micelles entering position 1 are the necessary condition in forming the aggregates; whereas, positions 2 and 3 are mandatory to construct the “pearl-necklace-like” morphology.

We would also like to understand quantitatively the formation mechanism of the “pearl-necklace-like” morphology. First, let us understand the electrostatic interactions. If we view the charged spherical micelle as a point charge with identical charges on all micelles, both in sign and in quantity, the electrical field strengths of positions 1, 2, and 3 can be calculated on the basis of Coulomb’s Law

$$\vec{E} = \left(\frac{kQ}{r^2} \right) \hat{r} \quad (1)$$

where E is the electrical field strength, r is the distance between charges, Q is the charge of the micelle, k is Coulomb’s constant, and \hat{r} is a unit vector in the radial direction. The magnitude of the electrical field at positions 1, 2, and 3, where it is assumed that each stationary micelle acts as a separate point charge, can be expressed as

$$E_1 = 0.433kQ/R_m^2, E_2 = 0.350kQ/R_m^2, E_3 = 0.312kQ/R_m^2$$

Here R_m is the radius of the spherical micelle. Because the electrostatic repulsion force is $F = QE$, it is evident that position 3 possesses the lowest electrostatic repulsion force;

whereas, position 1 has the highest one, assuming that Q and R_m are equal for all positions.

We can also consider this problem from the energy aspect. Through integration, we can calculate the electrical potential energy at the contact surface of the micelle

$$V_q = \int F \cdot dl \quad (2)$$

Values at the three different positions ($V_{q1} = kQ^2/R_m$, $V_{q2} = 0.85kQ^2/R_m$, and $V_{q3} = 0.75kQ^2/R_m$) can be obtained via the integration in eq 2. Again, position 1 has the highest threshold energy barrier, whereas position 3 has the lowest.

Now, we try to illustrate the hydrogen bonding energies and compare them with the electrical potential barriers. To calculate these energies, the first task is to know the surface area per chain occupied. The overall core surface of a spherical micelle (S_A) can be calculated as

$$S_A = 4\pi R_c^2 \quad (3a)$$

where R_c is the core radius of the micelle (where $R_c/R_m = (f_v^{PS})^{1/3}$). For the number of diblock polymers in a micelle (N), it can be expressed as

$$N = \frac{4/3\pi R_c^3 f}{V_S N_{PS}} \quad (3b)$$

where f is the PS volume fraction in the core, V_S is the volume of the PS monomer, and N_{PS} is the degree of polymerization of the PS blocks. Therefore, the interfacial area per chain S is

$$S = \frac{3V_S N_{PS}}{fR_c} \quad (3c)$$

The tethering density (σ) of the PEO blocks in the corona is the number of chains found in a unit surface area,^{38–44} whereby σ is the reciprocal of S

$$\sigma = 1/S \quad (4)$$

The reduced tethering density $\tilde{\sigma}$ can be expressed as

$$\tilde{\sigma} = \frac{\pi R_g^2}{S} \quad (5)$$

where R_g is the radius of gyration of the corona block, in this case, PEO. The reduced tethering density is utilized to describe the crowding of the corona PEO chains.²⁵

Hydrogen bonding occurs between PEO and PAA on a single micelle or between two micelles. The hydrogen bonding density (σ_H) must have a proportional relationship with the tethering density of PEO

$$\sigma_H = f_H \sigma \quad (6)$$

where f_H is the proportion coefficient for hydrogen bonding. Therefore, the hydrogen bonding energy (E_H) is expressed as below

$$E_H = \sigma_H S_H e_H \quad (7a)$$

where S_H is the hydrogen bonding area and e_H is the energy per hydrogen bond. The hydrogen bonding area is calculated as

$$S_H = 2\pi R_m h \quad (7b)$$

where h is the hydrogen bonding length, which is related to the contact area and distance of interaction between the PAA and the PEO corona.

To calculate the hydrogen bonding density and electrical charges on the micelle's surface, we need to analyze the adsorption and aggregation processes (Scheme 1) in detail. The first step is adsorption. As a reminder, the PAA is assumed to be completely adsorbed onto the PEO corona surface with each PAA monomer being accounted for within a single PEO chain area. Assuming that the fraction of hydrogen-bonded PEO sites per PEO block is r_1 , and the fraction of non-hydrogen-bonded PEO sites per PEO block is r_1' , we then have that

$$r_1 + r_1' = 1 \quad (8a)$$

The value of r_1 has a relationship with the reduced tethering density. With increased reduced tethering density, the corona PEO chains will be more crowded, leading to a smaller value of r_1 for each PEO block, namely, as the reduced tethering density increases, r_1 is reduced. When $\tilde{\sigma} = 1$, r_1 was considered to be < 0.5 . This assumption is based on a geometric consideration that the tethered corona PEO blocks adopt a random, spherical conformation on the core PS blocks and that they are touching at the outer edge.³⁸ We assume that a maximum probability of the PEO monomers in the blocks having an opportunity to interact with PAA is located in the upper-half of those spheres. This is equivalent to $r_1 = 0.5$. In general, however, the probability to interact with PAA must be smaller than this value of 0.5. As a first approximation, with immiscible tether and core blocks

$$r_1 \leq \frac{1}{2\tilde{\sigma}} \text{ when } 1 < \tilde{\sigma} < 3.7 \quad (8b)$$

As the conformation of the tethered chain changes after the transition into the interacting regime (or even the highly stretched regime), r_1 will have a stronger inverse relationship due to the decrease in available PEO area.^{38,39}

From the PAA standpoint, we assume that the fraction of hydrogen-bonded PAA sites with PEO in one PEO block area (complete adsorption) is r_2 , the fraction of non-hydrogen-bonded PAA sites within each PEO block area is r_2' , and the fraction of ionized PAA sites within each PEO block area is r_2'' , leading to

$$r_2 + r_2' + r_2'' = 1 \quad (9a)$$

Hydrogen bonding is directional, and the COOH groups in PAA are randomly distributed along the chains. Only part of the COOH groups can meet the geometric requirement to form a hydrogen bond with the PEO chain site on the micelle surface. Here we assume that the number of PAA sites involved in hydrogen bonding is almost equal to that of non-hydrogen-bonding sites ($r_2 \approx r_2'$).

Ionization equilibrium of non-hydrogen-bonded PAA monomers in aqueous solution must also be taken into account. According to ionization equilibrium, assuming that each section of PAA per PEO area is equal, we have

$$\log \frac{r_2'}{r_2''} = pK_{a(PAA)} - pH \quad (9b)$$

where $pK_{a(PAA)}$ is 5.6¹² and the pH value is 3.0. Therefore, the total number of PAA sites within one PEO block area becomes

$$N_{AA} = \frac{N_{PEO} r_1}{r_2} \quad (10)$$

where N_{PEO} is the degree of polymerization of the PEO block. The number of PAA sites available in each PEO block area after adsorption for further hydrogen bonding with secondary (adjacent) micelles during flocculation is

$$N_{\text{AA}'} = \frac{N_{\text{PEO}}r_1}{r_2} r_2' \quad (11)$$

The charge number in one PEO block area is

$$q_C = N_{\text{AA}''} = \frac{N_{\text{PEO}}r_1}{r_2} r_2'' \quad (12a)$$

Therefore, the overall charge per micelle should be

$$Q = 4\pi R_m^2 \sigma N_{\text{AA}''} \quad (12b)$$

To stabilize the micelle flocculation, there is a small amount of interpenetration between the contacting micelles. This results in intermicelle hydrogen-bonding. This can occur between the adsorbed PAA chains or the PAA chain of one micelle and the PEO of the adjacent micelle. In reference to the aggregation step as shown in Scheme 1, we assume that the fraction of AA-AA forming hydrogen bonding is r_3 , the fraction of AA-EO forming hydrogen bonding is r_3' , and the fraction of non-hydrogen bonding is r_3'' . The hydrogen-bonding number per PEO block area is thus

$$N_{\text{HC}} = f_H = \frac{N_{\text{PEO}}r_1}{r_2} r_2'(r_3 + r_3') \quad (13)$$

The total hydrogen bonding energy of the system thus becomes

$$E_H = \sigma \frac{N_{\text{PEO}}r_1}{r_2} r_2'(r_3 + r_3') S_{\text{HeH}} \quad (14a)$$

Because position 1 has two adjacent micelle contact areas whereas positions 2 and 3 only have one, the hydrogen bonding energy at position 1 is twice position 2 or 3

$$E_{\text{H1}} = 2E_H \quad (14b)$$

$$E_{\text{H2}} = E_H \quad (14c)$$

$$E_{\text{H3}} = E_H \quad (14d)$$

At pH 3.0, based on the above analysis, the electrical energy barriers and hydrogen bonding complexation free energies^{45,46} at different positions were estimated to be

$$E_{\text{q1}} = 4.8kT, E_{\text{q2}} = 4.1kT, E_{\text{q3}} = 3.6kT$$

$$E_{\text{H1}} = -16.6kT, E_{\text{H2}} = -8.3kT, E_{\text{H3}} = -8.3kT$$

where negative free energy indicates favorable interactions and positive free energy represents unfavorable interactions (attractive and repulsive, respectively). Because the flocculation is a dynamic process, the barrier of electrostatic repulsion is more important and over a larger length scale than the energy of attraction for hydrogen-bonding. As such, the E_{q} values are more representative for the formation of the “pearl-necklace-like” structure. It should also be noted that

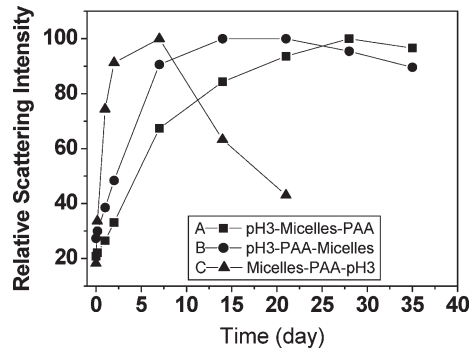


Figure 7. LLS of the micelles aggregation process at pH 3.0 after 1 h of association filtered with 1 μm syringe filter.

the hydrogen-bonding distance, h , may be smaller for position 1, which would result in a lower value for E_{H1} . These calculations quantitatively demonstrate the energy barriers at the different positions. Position 3 has the lowest energy barrier, which favors “pearl-necklace-like” morphology. At the same time, once the aggregation happens, the hydrogen bonding does possess enough energy to stabilize the aggregation.

It has also been reported that the “pearl-necklace-like” or even cylindrical morphology can be observed via extrusion of PS-block-polyisoprene spherical micelles in solution through a “nano-channel” constructed by a double-layered membrane. The diameter of the channel is smaller than that of the sphere micelles. These spherical micelles are thus squeezed, aligned, and connected in the “channel”.⁴⁷ In that case, the formed “pearl-necklace-like” or cylindrical morphology is in an unstable, nonequilibrium state. Ultimately, the micelles separate again to become individual spheres. In our case, this type of “pearl-necklace-like” morphology formed spontaneously and thus from a thermodynamic point-of-view is in at least a metastable state with a free energy minimum.

Aggregation Formation and Kinetics at pH 3. We utilized LLS to monitor further the complexation process at pH 3.0. In our original experimental approach, we diluted the original micelles in a pH 3.0 water solution and added PAA solution (abbreviated as pH3-Micelles-PAA). To understand the formation pathway, for comparison, we designed two other approaches to generate the complex. In one case, we added the PAA into a pH 3.0 water solution and then added the micelles (abbreviated as pH3-PAA-micelles). In another, we mixed the PAA and the micelles in neutral DI water and adjusted the pH value to 3.0 by titration (abbreviated as micelles-PAA-pH3).

LLS results in Figure 7 show that the micelles-PAA-pH3 procedure exhibits the fastest aggregation rate (increased intensity). After several days, the scattering intensity reached a maximum and then subsequently decreased. The scattering intensity decrease indicates that the aggregate is large and starts to precipitate out of solution. The pH3-micelles-PAA procedure is the slowest among these three, and it requires almost 30 days to reach the maximum. If we wait for a time period that is long enough, then the scattering intensity will eventually decrease. The procedure of pH3-PAA-micelles needs about 15 to 20 days to form large aggregates, as shown in Figure 7.

The micelles-PAA-pH3 procedure is the fastest because of the fact that during the titration process to adjust (decrease) the pH value, there are some locations where locally a few droplets at lower pH have not dispersed to reach the average pH value. Because we know that at a pH value lower than 3.0

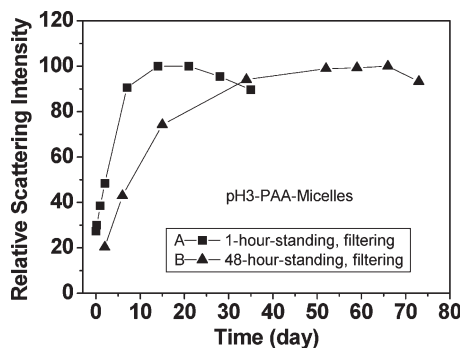


Figure 8. LLS of the aggregation process after different standing time: (A) 1 h of standing and filtering and (B) 48 h of standing and filtering.

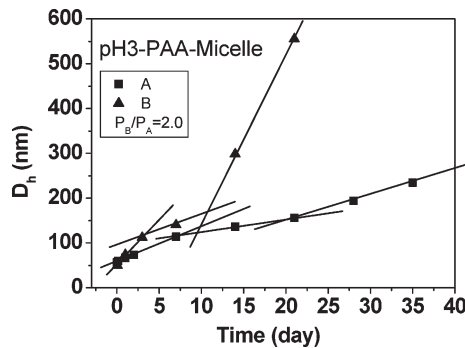


Figure 9. Hydrodynamic diameter growth for pH3-PAA-micelles. The population of micelles in B (P_B) is different than the population of micelles in A (P_A).

the flocculation kinetics speeds up (Figure 6), these locations may thus form local aggregates acting as nuclei for further development. As for the other two samples, the procedure of pH3-PAA-micelles is faster than that of pH3-micelles-PAA. This is because the PAA has reached the lower ionization value prior to the addition of the micelles, which facilitates the adsorption process. In pH3-micelles-PAA, the decrease in ionization of PAA must happen to allow adsorption of the PAA onto the micelle before flocculation.

To understand qualitatively the effect of the initial nuclei and micelle concentration on the aggregation process, we monitored the aggregation under different starting conditions. Experimental samples were evaluated after 1 h of association and subsequent filtering or after 48 h of association and filtering. They were then monitored using LLS. The results are shown in Figure 8. After 1 h of association, the aggregation is still small, and only a few have been filtered out. However, after 48 h of association, the aggregates were large enough to be removed by the filter. After 48 h, the number of aggregate nuclei and the overall micelle population are much less than after 1 h; therefore, after the removal of larger aggregates, further aggregation must be very slow. Therefore, it takes a long period of time for the LLS intensity to reach the maximum in the 48 h sample.

Figure 9 shows the growth of the hydrodynamic diameter of the aggregation detected by LLS. Two sets of data (A and B) are included. They were both prepared after 1 h of association and filtering but have different micelle populations. B is about twice that of A. The growth of the hydrodynamic diameter in B is faster than that in A. In both A and B, we can clearly observe the three stages of aggregation. Initially, the growth rate was high, but it then slows down. At longer times, there was another acceleration region. TEM images shown in Figure 10 exhibit the morphologies in

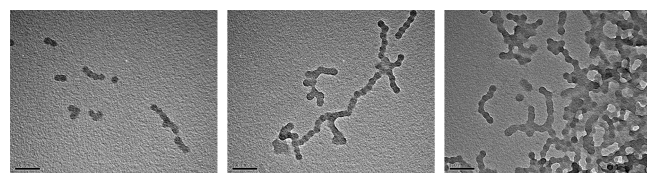


Figure 10. TEM image of association behavior at pH 3.0 in different stages: (a) early stage, (b) middle stage, and (c) late stage. The scale bar is 100 nm.

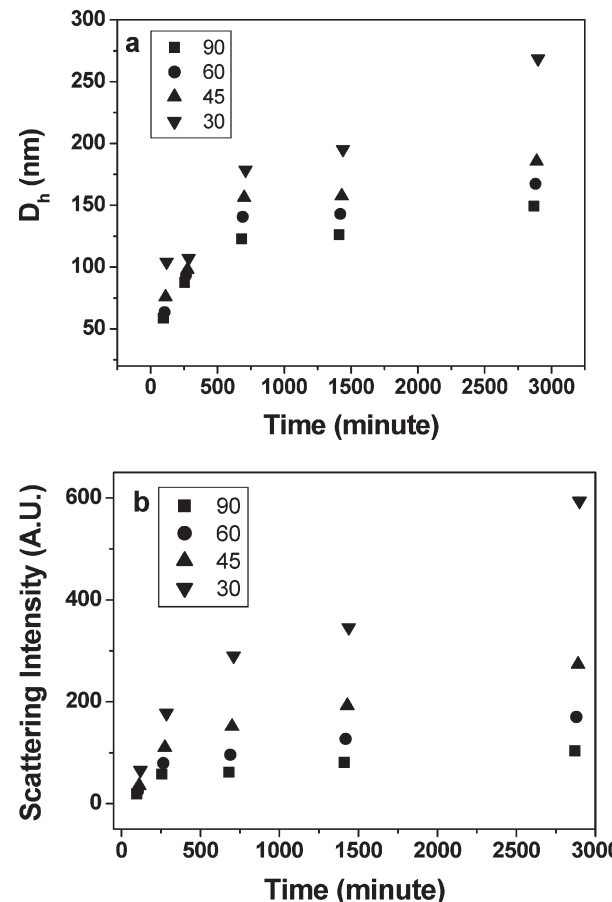


Figure 11. Dynamic LLS results in monitoring (a) the hydrodynamic diameter changes and (b) the scattering intensity changes at different scattering angles and times of the complexation for PAA-micelles-pH3. Before the complexation, the PAA and acidic solutions were filtered by $0.1\text{ }\mu\text{m}$ filter, whereas the micelle solution was filtered by $0.45\text{ }\mu\text{m}$ filter.

different stages from left to right: the initial aggregation nuclei, the growth, and finally, the flocculation. Furthermore, we also examined the size and shape changes during the aggregation process by utilizing different scattering angles of LLS between 30 and 90°. Figures 11a,b illustrates the dynamic LLS of both the hydrodynamic diameter and scattering intensity, respectively, and their dependence on scattering angle. It is evident that in the early and middle stages of the aggregation process, asymmetric aggregates possess a broad size distribution that are caused by mixtures of the spherical micelle, the different length necklace-like aggregates, and the large aggregates. On the basis of our TEM result in Figures 6 and 10, the characteristic necklace-like morphologies appear on a time scale of 1 to 2 h, where the hydrodynamic diameter and intensity shown in Figure 11a,b exhibit strong scattering angle dependencies.

Aggregation is a very complicated process. On the basis of the LLS data, we can discuss the aggregation kinetics qualitatively. In this stage, only general cases can be written. For example, to form an aggregate, two primary micelles collide and stick together to form a doublet based on Brownian motion under electrostatic and hydrogen-bonding interactions. The subsequent kinetics of ionization and aggregation will also affect the ability of the molecules to adsorb and flocculate. A detailed kinetic description requires a detailed microscopic model and mechanism.

Conclusions

In summary, by precisely controlling the quantity and feeding rate of water into DMF solution of the PS₂₄₀-*b*-PEO₁₈₂ diblock copolymer, spherical micelles can be prepared with the PEO blocks located in the corona. The micelle association with PAA is pH-dependent and can be divided into three major regions: flocculation (when pH < 3.0), single sphere adsorption (when pH 3.0 to 4.8), and no adsorption (when pH > 4.8). The value of pH 3.0 has been recognized as the onset point of flocculation. The association of micelles is caused by hydrogen bonding between the PEO blocks and PAA chains without changing the shape of the micelles. At low pH values (pH < 3.0), the introduction of PAA into the system results in rapid flocculation. However, within 3.0 < pH < 4.8, feeding PAA is favored for dispersing the micelles, evidenced by a more negative ζ -potential compared with the micelles in neutral water. The complexation kinetics and aggregation mechanism in forming the “pearl-necklace-like” morphology are investigated when the pH value is equal to 3. The balance between hydrogen bonding and the electrostatic repulsion (and relevant surface charges) is attributed to the micelles stability and leads to the observation of the pH dependence of the association between the PS₂₄₀-*b*-PEO₁₈₂ micelles and PAA chains. The mechanism of forming the “pearl-necklace-like” morphology at pH 3.0 has also been discussed.

Acknowledgment. This work was supported by the National Science Foundation (DMR-0906898).

References and Notes

- (1) Hamley, I. W. *Block Copolymer in Solution: Fundamentals and Applications*; John Wiley & Sons: Chichester, England, 2005.
- (2) Tuzar, Z.; Kratochvil, P. *Adv. Colloid Interface Sci.* **1976**, *6*, 201.
- (3) Tuzar, Z.; Kratochvil, P. In *Surface Colloid Science*; Matijevic, E., Ed.; Plenum: New York, 1993; Vol. 15, 1.
- (4) Riess, G. *Prog. Polym. Sci.* **2004**, *28*, 1107.
- (5) Förster, S.; Plantenberg, T. *Angew. Chem., Int. Ed.* **2002**, *41*, 688.
- (6) Liu, S.; Armes, S. P. *Curr. Opin. Colloid Interface Sci.* **2001**, *6*, 249.
- (7) Cheng S. Z. D. *The Phase Transitions in Polymers: The Role of Metastable States*; Elsevier: Amsterdam, The Netherlands, 2008.
- (8) Hamely, I. W. *Introduction to Soft Matter: Polymers, Colloids, Amphiphiles and Liquid Crystals*; John Wiley & Sons: Chichester, England, 2009.
- (9) Dorby, A. *Bull. Soc. Chim. Belg.* **1948**, *57*, 280.
- (10) Bailey, F. E.; Lundberg, R. D.; Callard, R. W. *J. Polym. Sci., Part A: Polym. Chem.* **1964**, *2*, 845.
- (11) Bailey, F. E.; Koleske, J. V. *Poly(ethylene oxide)*; Academic Press: New York, 1976.
- (12) Tsuchida, E.; Abe, J. *Adv. Polym. Sci.* **1982**, *45*, 1.
- (13) Jiang, M.; Li, M.; Xiang, M.; Zhou, H. *Adv. Polym. Sci.* **1999**, *146*, 121.
- (14) Gao, W.; Bai, Y.; Chen, E.; Li, Z.; Han, B.; Yang, W.; Zhou, Q. *Macromolecules* **2006**, *39*, 4894.
- (15) Bai, Y.; Gao, W.; Yan, J.; Ma, Y.; Liang, D.; Li, Z.; Han, B.; Yang, W.; Chen, E. *Polymer* **2008**, *49*, 2099.
- (16) Xie, D.; Xu, K.; Bai, R.; Zhang, G. *J. Phys. Chem. B* **2007**, *111*, 778.
- (17) Xie, D.; Bai, W.; Xu, K.; Bai, R.; Zhang, G. *J. Phys. Chem. B* **2007**, *111*, 8034.
- (18) Karanikolas1, A.; Tsolakis, P.; Bokias, G.; Tsitsilianis1, C. *Eur. Phys. J. E* **2008**, *27*, 335.
- (19) Lee, C. H.; Ho, K. M.; Harris, F. W.; Cheng, S. Z. D.; Li, P. *Soft Matter* **2009**, *5*, 4914.
- (20) Quirk, R. P.; Kim, J.; Kausch, C.; Chun, M. S. *Polym. Int.* **1996**, *39*, 3.
- (21) Zhu, L.; Cheng, S. Z. D.; Calhoun, B. H.; Ge, Q.; Quirk, R. P.; Thomas, E. L.; Hsiao, B. S.; Yeh, F.; Lotz, B. *Polymer* **2001**, *42*, 5829.
- (22) McGoman, J. C. *Polymer* **1969**, *10*, 841.
- (23) Zhang, L.; Eisenberg, A. *Science* **1995**, *268*, 1728.
- (24) Yu, K.; Eisenberg, A. *Macromolecules* **1996**, *29*, 6359.
- (25) Bhargava, P.; Zheng, J. X.; Li, P.; Quirk, R. P.; Harris, F. W.; Cheng, S. Z. D. *Macromolecules* **2006**, *39*, 4880.
- (26) Bhargava, P.; Zheng, J. X.; Quirk, R. P.; Cheng, S. Z. D. *J. Polym. Sci., Polym. Phys. Ed.* **2006**, *44*, 3605.
- (27) Bhargava, P.; Tu, Y.; Zheng, J. X.; Xiong, H.; Quirk, R. P.; Cheng, S. Z. D. *J. Am. Chem. Soc.* **2007**, *129*, 1114.
- (28) Chu, B. *Laser Light Scattering: Basic Principles and Practice*, 2nd Ed.; Academic Press: San Diego, CA, 1991.
- (29) Evans, D. F.; Wennerström, H. *The Colloidal Domain, Where Physics, Chemistry, Biology, and Technology Meet*; Wiley-VCH: New York, 1999; Chapter 3.
- (30) Choi, J.; Rubner, M. F. *Macromolecules* **2005**, *38*, 116.
- (31) Xie, A. F.; Granick, S. *Macromolecules* **2002**, *35*, 1805.
- (32) Sukhishvili, S. A.; Granick, S. *Macromolecules* **2002**, *35*, 301.
- (33) Delongchamp, D. M.; Hammond, P. T. *Langmuir* **2004**, *20*, 5403.
- (34) Yang, S.; Zhang, Y.; Zhang, X.; Xu, J. *Soft Matter* **2007**, *3*, 463.
- (35) Bokias, G.; Staikos, G.; Iliopoulos, I.; Audebert, R. *Macromolecules* **1994**, *27*, 427.
- (36) Daniel, J. C.; Audebert, R. In *Soft Matter Physics*; Daoud, M., Williams, C. E., Eds.; Springer-Verlag: Berlin, 1999; Chapter 3.
- (37) Davidson, R. L. *Handbook of Water-Soluble Gums and Resins*; McGraw-Hill: New York, 1980; pp 17–3.
- (38) Chen, W. Y.; Zheng, J. X.; Cheng, S. Z. D.; Li, C. Y.; Huang, P.; Zhu, L.; Xiong, H.; Ge, Q.; Guo, Y.; Quirk, R. P.; Lotz, B.; Deng, L.; Wu, C.; Thomas, E. L. *Phys. Rev. Lett.* **2004**, *93*, 028301.
- (39) Zheng, J. X.; Xiong, H.; Chen, W. Y.; Lee, K.; Van Horn, R. M.; Quirk, R. P.; Lotz, B.; Thomas, E. L.; Shi, A.-C.; Cheng, S. Z. D. *Macromolecules* **2006**, *39*, 641.
- (40) Hsiao, M.-S.; Zheng, J. X.; Van Horn, R. M.; Quirk, R. P.; Thomas, E. L.; Chen, H.-L.; Lotz, B.; Cheng, S. Z. D. *Macromolecules* **2009**, *42*, 8343.
- (41) Taunton, H. J.; Toprakcioglu, C.; Fetter, L. J.; Klein, J. *Nature* **1988**, *332*, 712.
- (42) Granick, S.; Herz, J. *Macromolecules* **1985**, *18*, 460.
- (43) Kent, M. S.; Lee, L. T.; Farnoux, B.; Rondelez, F. *Macromolecules* **1992**, *25*, 6240.
- (44) Bhushan, B.; Israelachvili, J. N.; Landman, U. *Nature* **1995**, *374*, 607.
- (45) Osada, Y. *J. Polym. Sci., Polym. Chem. Ed.* **1979**, *17*, 3485.
- (46) Tsuchida, E.; Osada, Y.; Ohno, H. *J. Macromol. Sci., Phys.* **1980**, *B17*, 683.
- (47) Chen, Q.; Zhao, H.; Ming, T.; Wang, J.; Wu, C. *J. Am. Chem. Soc.* **2009**, *131*, 16650.